Developmental regression of hyaloid vasculature is triggered by neurons

Yusuke Yoshikawa,[1,2]* Toru Yamada,[1,2]* Ikue Tai-Nagara,[1] Keisuke Okabe,[1,3] Yuko Kitagawa,[2] Masatsugu Ema,[4] and Yoshiaki Kubota[1]

[1]Department of Vascular Biology, The Sakaguchi Laboratory, [2]Department of Surgery, and [3]Department of Plastic Surgery, School of Medicine, Keio University, Shinjuku-ku, Tokyo 160-8582, Japan
[4]Department of Stem Cells and Human Disease Models, Research Center for Animal Life Science, Shiga University of Medical Science, Tsukinowa-cho, Otsu 520-2192, Japan

Vascular development involves not only vascular growth, but also regression of transient or unnecessary vessels. Hyaloid vasculature is the temporary circulatory system in fetal eyes, which spontaneously degenerates when the retinal blood vessels start to grow. Failure of the hyaloid vessels to regress leads to disease in humans, persistent hyperplastic primary vitreous, which causes severe intraocular hemorrhage and impairs visual function. However, the mechanism underlying the endogenous program that mediates spontaneous regression of the hyaloid vessels is not well understood. In this study, we identify a robust switch triggering this program directed by neurons in mice. Marked up-regulation of vascular endothelial growth factor (VEGF) receptor 2 (VEGFR2) occurs in retinal neurons just after birth via distal-multipotent-mesodermal enhancer, a hemangioblast-specific enhancer of VEGFR2. Genetic deletion of neuronal VEGFR2 interrupts this program, resulting in massive hyaloid vessels that persist even during late postnatal days. This abnormality is caused by excessive VEGF proteins in the vitreous cavity as a result of impairment in the neuronal sequestration of VEGF. Collectively, our data indicate that neurons trigger transition from the fetal to the postnatal circulatory systems in the retina.

The Journal of Experimental Medicine

Vascular development involves not only vascular growth (sprouting, proliferation, and branching), but also regression of established blood vessels (Potente et al., 2011). The hyaloid vasculature is a temporary circulatory system formed in the eyes of a fetus that immediately regresses after birth in mice and by the fifth month of gestation in humans as the growing retinal vasculature takes over the role of the hyaloid vasculature to supply oxygen and nutrients to retinal tissues (Lang and Bishop, 1993; Silbert and Gurwood, 2000). In humans, failure of the hyaloid vessels to regress leads to an ocular pathology called persistent hyperplastic primary vitreous (PHPV), which causes severe intraocular hemorrhage and impairs visual function (Silbert and Gurwood, 2000). This programmed regression of hyaloid vessels is partly controlled by macrophages that secrete factors that mediate cell death in the endothelium, such as Wnt7b (Lang and Bishop, 1993; Lobov et al., 2005). Here, we show that this switch is also triggered by another process orchestrated by neurons. Our data indicate that retinal neurons ultimately control the precise switch from the fetal to the postnatal circulatory systems by timely sequestering vascular endothelial growth factor (VEGF).

RESULTS AND DISCUSSION

Neuronal VEGF expression correlates with the number of hyaloid vessels

Our first step was to reliably visualize the entire hyaloid vessel structure. For this purpose, we isolated the hyaloid vessels en bloc with the iris, which acted as a frame (Fig. 1 A). Using this technique, we succeeded in visualizing the hyaloid vasculature together with the associated macrophages (Fig. 1, B–D). We also detected spontaneous endothelial apoptosis and vascular regression marked by collagen IV$^+$ vascular endothelial cadherin$^-$ cord-like structures (Fig. 1, E–G). In agreement with a previous study (Rao et al., 2013), hyaloid vessels did not grow after postnatal day 3 (P3) and were almost completely regressed before P12 (Fig. 1, H–J).

Retinal neurons contribute to the formation of retinal vessels both in physiological and pathological conditions (Sapieha et al., 2008; Usui et al., 2015). Retinal neurons are also suggested to act on hyaloid vasculature (Xu et al., 2004; Kurihara et al., 2010), in part by secreting VEGF (Rao et al., 2013). Therefore, we generated mice lacking *Vegfa* in retinal neurons using *Pax6α-Cre* or *Chx10-Cre*. The Cre recombination for *Pax6a-Cre* occurs in the peripheral area of retinas (Marquardt et al., 2001), whereas it occurs for *Chx10-Cre* in all retinal neurons (Fig. 1, K and L). The Cre recombinase was not active in endothelial cells and macrophages in hyaloid

*Y. Yoshikawa and T. Yamada contributed equally to this paper.

Correspondence to Yoshiaki Kubota: ykubo33@a3.keio.jp

Abbreviations used: BAC, bacterial artificial chromosome; DMME, distal-multipotent-mesodermal enhancer; PHPV, persistent hyperplastic primary vitreous; VEGF, vascular endothelial growth factor.

The Rockefeller University Press $30.00
J. Exp. Med. 2016 Vol. 213 No. 7 1175–1183
www.jem.org/cgi/doi/10.1084/jem.20151966

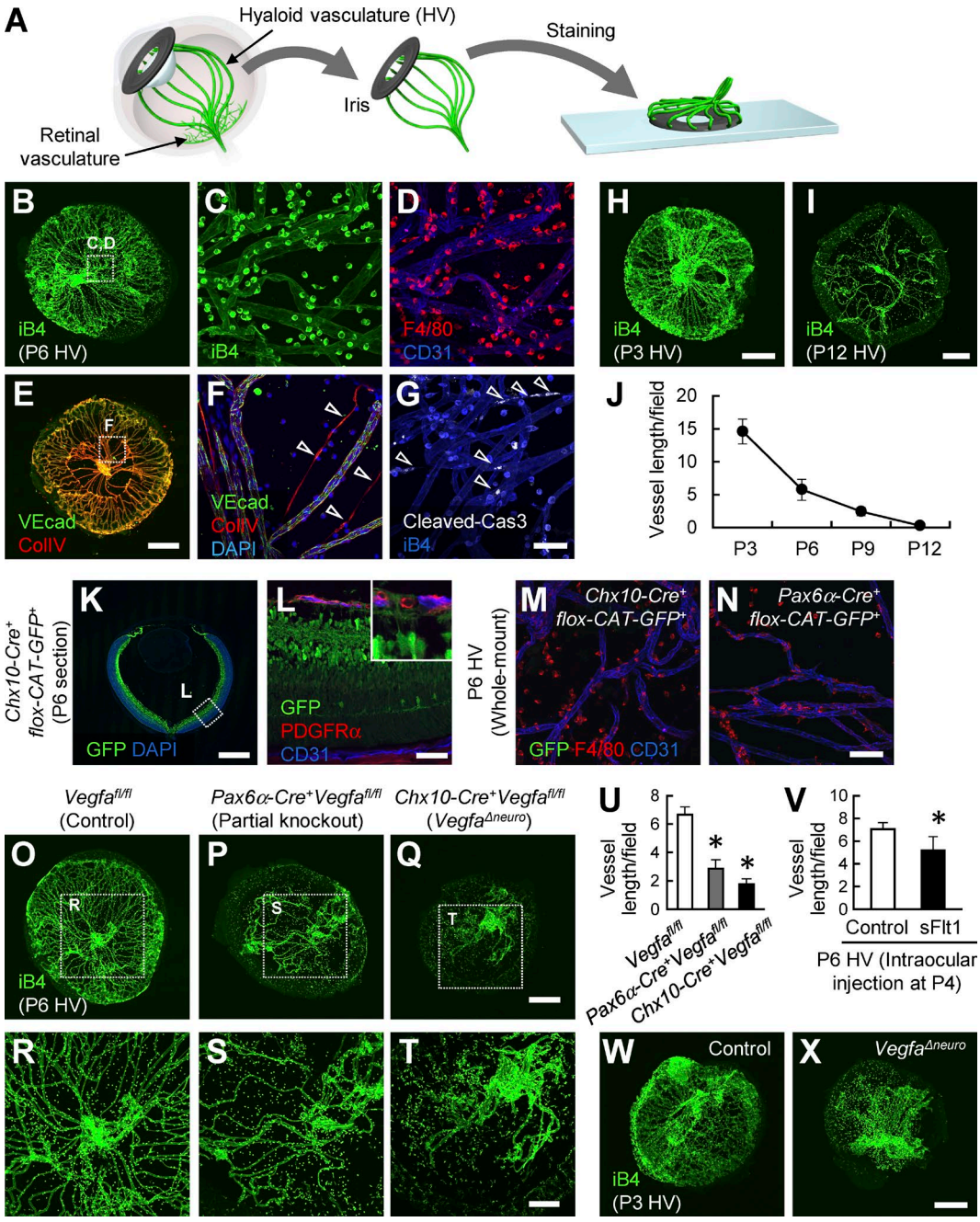

Figure 1. **Neuronal VEGF expression correlates with the number of hyaloid vessels.** (A) Schematic diagram depicting the technique used to visualize the hyaloid vasculature. (B–J) Whole-mount stained images of hyaloid vessels at P3, P6, or P12 and quantification ($n = 4$). Spontaneous vessel regression (arrowheads in F) and apoptosis (arrowheads in G) are indicated. VEcad, vascular endothelial cadherin. (K–X) Immunohistochemical images of a retinal section (K and L) and hyaloid vessels (M–T, W, and X) and quantification ($n = 4$). Bars: (B, E, H, I, K, O–Q, W, and X) 500 µm; (R–T) 200 µm; (C, D, F, G, and L–N) 50 µm. *, $P < 0.05$; two-tailed Student's *t* tests. Representative confocal images from four independent experiments (four mice per group) are shown. Data are represented as mean ± SD. CAT, chloramphenicol acetyltransferase; PDGFRα, platelet-derived growth factor receptor α.

vessels in these lines (Fig. 1, M and N). The resultant conditional knockout mice showed significantly reduced hyaloid vessels compared with control mice at P6 (Fig. 1, O–U). Reflecting the difference in the extent of the Cre recombination, the phenotype was more severe in *Chx10-Cre*$^{+}$*Vegfa*$^{flox/flox}$ (*Vegfa*$^{\Delta neuro}$) than in *Pax6α-Cre*$^{+}$*Vegfa*$^{flox/flox}$ mice. Intraocular injection of Flt1-Fc chimeric proteins, which bind and inactivate VEGF proteins, accelerated the hyaloid vessel regression (Fig. 1 V). In contrast, *Vegfa*$^{\Delta neuro}$ showed greatly reduced hyaloid vessels compared with control mice at P3 (Fig. 1, W and

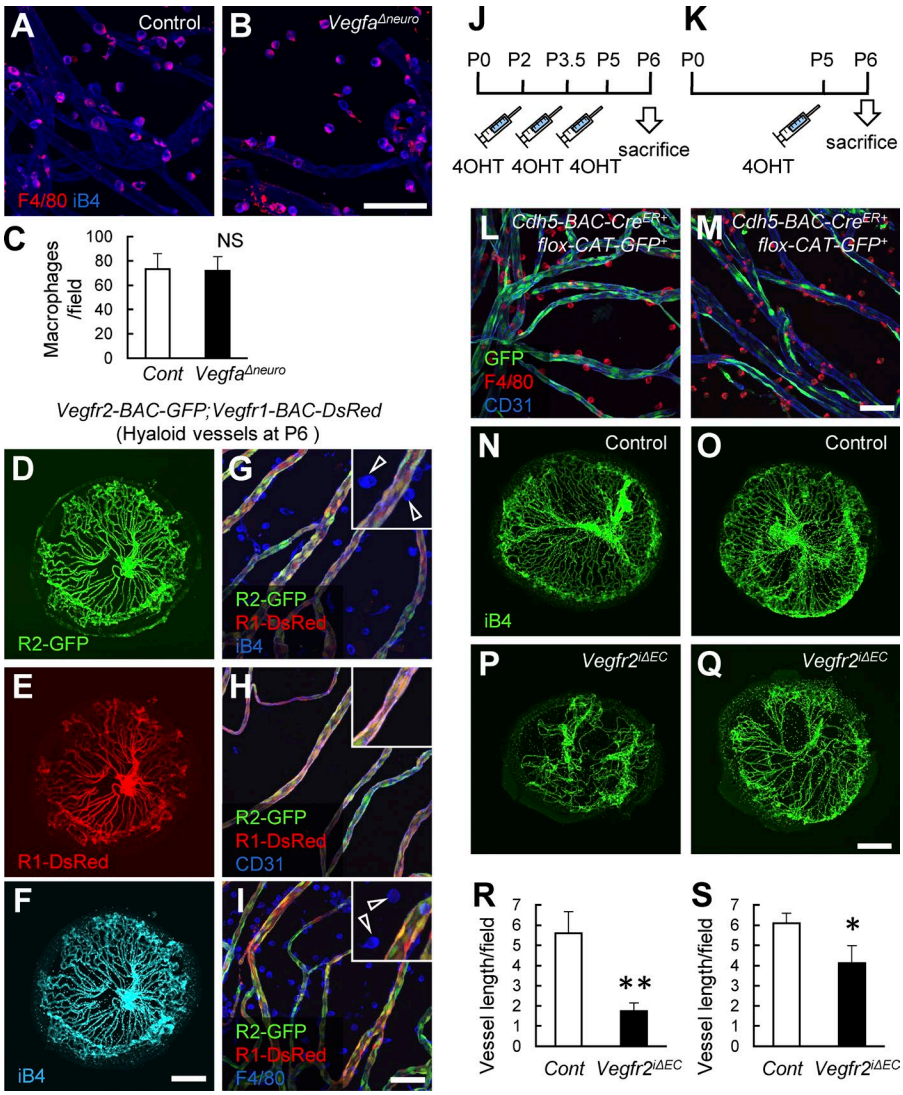

Figure 2. **VEGF maintains hyaloid vessels via endothelial VEGFR2.** (A–C) Whole-mount stained images of hyaloid vessels at P6 and quantification (n = 4). (D–I) Whole-mount stained images of hyaloid vessels at P6. Neither *Vegfr1* nor *Vegfr2* is detected in macrophages (arrowheads in G and I). (J and K) Schematic diagram depicting the timing of 4-hydroxytamoxifen (4OHT) injections. (L–S) Whole-mount stained images of hyaloid vessels at P6 and quantification (n = 4). Bars: (D–F and N–Q) 500 µm; (A, B, G–I, L, and M) 50 µm. *, $P < 0.05$; **, $P < 0.01$; two-tailed Student's t tests. Representative confocal images from four independent experiments (four mice per group) are shown. Data are represented as mean ± SD. CAT, chloramphenicol acetyltransferase; Cont, control.

X) when the hyaloid vessels started to regress, suggesting that VEGF signaling is associated with the formation of hyaloid vessels as well as their maintenance.

VEGF maintains hyaloid vessels via endothelial VEGFR2

Based on existing data, we suspected that the *Vegfa*$^{\Delta neuro}$ mouse phenotype could be attributed to VEGF actions on macrophages. Therefore, we first determined the number and morphology of macrophages associated with hyaloid vessels but found no difference between control and *Vegfa*$^{\Delta neuro}$ mice (Fig. 2, A–C). Using bacterial artificial chromosome (BAC)–transgenic mice (Ishitobi et al., 2010), we detected expression of VEGF receptor 1 (VEGFR1) and VEGFR2 in endothelial cells, whereas their reporter activities in macrophages were below detectable levels (Fig. 2, D–I). We then generated tamoxifen-inducible endothelial-specific VEGFR2 knockout mice (*Vegfr2*$^{i\Delta EC}$) by using *Cdh5-BAC-Cre*^{ERT2} (Okabe et al., 2014). We found that tamoxifen treatment after P2 in mutant mice markedly reduced the number of hyaloid vessels at P6, similar to what was observed in *Vegfa*$^{\Delta neuro}$ mice (Fig. 2, J, L, N, P, and R). Moreover, a single tamoxifen injection 24 h before sacrifice at P6 was sufficient to significantly reduce hyaloid vessels (Fig. 2, K, M, O, Q, and S). These data suggest that the regression rate of hyaloid vessels highly depends on endothelial VEGFR2 signaling.

VEGFR2 is markedly up-regulated via distal-multipotent-mesodermal enhancer (DMME) in retinal neurons after birth

Because neuronal VEGF is essential for hyaloid vasculature maintenance, we hypothesized that the timed regression of hyaloid vessels after birth might be caused by physiological down-regulation of neuron-derived VEGF. However, the results of our quantitative PCR analysis indicated that *Vegfa* expression was not significantly different before and after birth (Fig. 3, A and B). Immunohistochemistry of retinal sections confirmed that VEGF proteins were constantly detected in

retinal neurons, although expression levels gradually decreased 2 wk after birth (Fig. 3, D–H). The abundant expression of VEGF proteins in the outer segments of adult eyes is in agreement with the strong expression of VEGF genes in the retinal pigment epithelium (Saint-Geniez et al., 2006). In contrast, *Vegfr2* expression was markedly up-regulated immediately after birth (Fig. 3 C). Because retinal neurons are the major source of VEGFR2 in neonatal retinas (Okabe et al., 2014), we compared embryonic and neonatal retinas derived from *Vegfr2-BAC-GFP* mice. Importantly, we found that VEGFR2 expression in embryonic retinas was much weaker than that in P1 retinas (Fig. 3, I–P). DMME is a recently discovered hemangioblast-specific enhancer of VEGFR2, which contains Gata-, Cdx-, Tcf/Lef-, ER71/Etv2-, and Fox-binding sites (Ishitobi et al., 2011). We recently found that DMME is activated in neonatal neurons but not endothelial cells in the retina (Okabe et al., 2014). Here, using transgenic mice carrying the DMME-GFP transgene (Ishitobi et al., 2011), we found that DMME activity was abundant in the neurons of P1 retinas but below detectable levels in embryonic retinas (Fig. 3, Q and R). To determine whether DMME activation is functionally involved in the neonatal up-regulation of VEGFR2 in neurons, we analyzed VEGFR2 expression in mice lacking DMME (*Vegfr2*$^{\Delta DMME/DMME}$). The peripheral half of the retina at P2, which does not contain endothelial components, showed one third the expression of *Vegfr2* in *Vegfr2*$^{\Delta DMME/DMME}$ compared with that in wild-type pups (Fig. 3 S). This low *Vegfr2* expression still remaining in the *Vegfr2*$^{\Delta DMME/DMME}$ retina indicated that a regulatory mechanism other than DMME maintains baseline expression of VEGFR2 in retinal neurons.

Lack of neuronal VEGFR2 leads to persistent hyaloid vessels

To examine the roles of neuronal VEGFR2, we generated mice lacking VEGFR2 in retinal neurons using *Chx10-Cre* (*Vegfr2*$^{\Delta neuro}$). The density of the hyaloid vasculature in the resulting mutant mice was much greater than that in control mice at P6 (Fig. 4, A–F and O). Although the amount of hyaloid vessels present did not differ between control and *Vegfr2*$^{\Delta neuro}$ at P3, the dense network of hyaloid vessels in the *Vegfr2*$^{\Delta neuro}$ mouse persisted even at P12, a time when hyaloid vessels are normally almost completely diminished (Fig. 4, M–O; unpublished data). This time course in vascular density indicated that the defect in the hyaloid vasculature in the *Vegfr2*$^{\Delta neuro}$ mouse was attributable to impaired regression but not increased formation. Although macrophage numbers were not changed, endothelial apoptosis and vascular regression were markedly reduced in *Vegfr2*$^{\Delta neuro}$ mice (Fig. 4, G–L, P, and Q). The neuronal integrity and morphology were intact in *Vegfr2*$^{\Delta neuro}$ mice (unpublished data). *Vegfr2*$^{\Delta DMME/DMME}$ mice showed a slight but significant increase in the number of hyaloid vessels at P6 (Fig. 4 R), reflecting their low *Vegfr2* expression. Premature intraretinal vascularization, as seen in the peripheral retinas of mice with a *Pax6α-Cre*–mediated *Vegfr2* deletion (Okabe et al., 2014), was observed in all areas of the retina in *Vegfr2*$^{\Delta neuro}$ mice (Fig. 4, S–W).

Deletion of VEGF normalizes persistent hyaloid vessels in neuronal VEGFR2 knockout mice

Because increased VEGF production from retinal neurons is suggested to cause persistence of hyaloid vessels in Frizzled-4–deficient mice (Rattner et al., 2014), we measured the VEGF protein level in *Vegfr2*$^{\Delta neuro}$ mice. Importantly, we found markedly increased VEGF protein levels in the vitreous cavity of *Vegfr2*$^{\Delta neuro}$ mice (Fig. 5 B), whereas the mRNA level of *Vegfa* was not changed (Fig. 5 A). It is possible that the lack of soluble VEGFR2 (sVEGFR2), formed by a splice variant of the *Vegfr2* gene (Albuquerque et al., 2009), could increase the level of vitreous VEGF proteins, resulting in persistent hyaloid vessels. Therefore, we examined mice lacking sVEGFR2 but not membrane-bound VEGFR2 (*Vegfr2*$^{\Delta s/\Delta s}$). The results showed that lack of sVEGFR2 did not affect hyaloid vessels (Fig. 5, C and D), suggesting that sequestration of VEGF by sVEGFR2 is not associated with this process. Next, we generated mice lacking both *Vegfa* and *Vegfr2* in retinal neurons (*Vegfa*; *Vegfr2*$^{\Delta neuro}$). We found that deleting neuronal *Vegfa* normalized persistent hyaloid vessels and the absence of spontaneous endothelial apoptosis in *Vegfr2*$^{\Delta neuro}$ mice (Fig. 5, E–O).

Collectively, we identified a switch of the timed regression of hyaloid vessels. Neonatal but not embryonic neurons sequester VEGF protein in the vitreous cavity through binding to VEGFR2, causing endothelial apoptosis, switching the eyes from a fetal to a postnatal circulatory system (Fig. 5 P).

In terms of the pupillary membrane, another transient circulatory system in fetal eyes (Lang and Bishop, 1993), the phenotype was not apparent in *Vegfr2*$^{\Delta neuro}$ mice (unpublished data). We speculate that the soluble form of VEGFR1, known to be expressed in the cornea (Ambati et al., 2006), might be important for the sequestration of VEGF that leads to the regression of the pupillary membrane.

In humans, bilateral PHPV occurs in patients with Norrie disease, which is caused by a mutation in genes coding for the proteins involved in the signaling complex for Norrin (Ye et al., 2010). Interestingly, mice lacking Norrin show abundant up-regulation of VEGF in neurons, and blocking VEGF corrected the vascular defects in those mice (Xu et al., 2004; Wang et al., 2012; Rattner et al., 2014). Our present data fully support this scenario: persistent hyaloid vessels are ascribed to increased VEGF protein levels, occurring through either their overproduction or defective sequestration of VEGF by neurons.

Finally, our data identified that neuronal VEGF sequestering triggers the programmed regression of hyaloid vessels. It will be interesting to determine whether this mechanism holds true for the human pathology in PHPV.

MATERIALS AND METHODS

Mice. All procedures involving animals were approved by the Institutional Animal Care and Use Committee of Keio University and performed in accordance with the Guidelines of Keio University for Animal and Recombinant DNA Experiments. *Chx10-Cre* mice (Muranishi et al., 2011) or *Pax6α-Cre* mice (provided by P. Gruss, Max

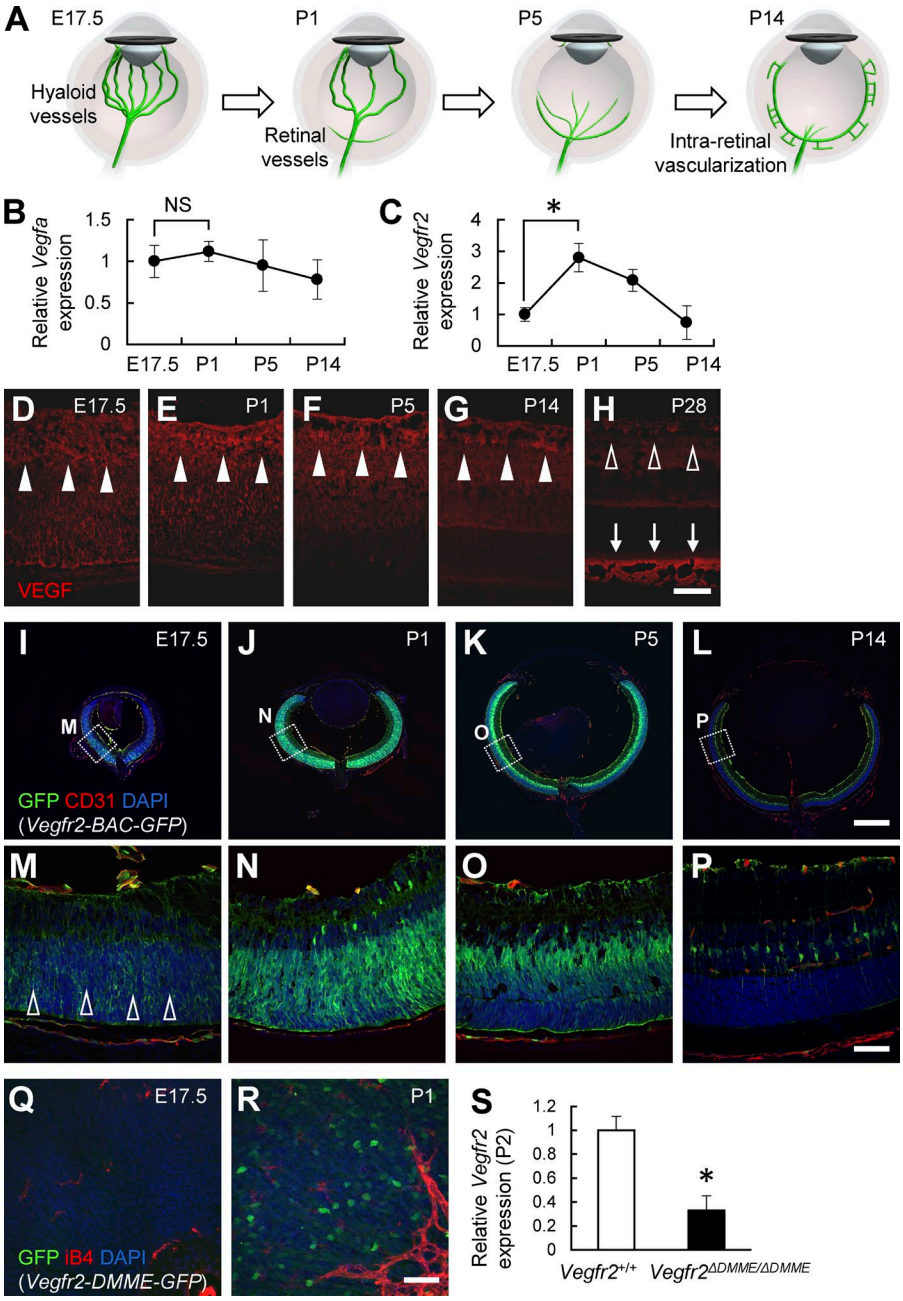

Figure 3. **VEGFR2 is markedly up-regulated via DMME in retinal neurons after birth.** (A) Schematic diagram depicting the developmental transition of the ocular circulatory system. (B and C) Quantitative PCR analysis of retinas at P6 (n = 4). (D–P) Immunohistochemical analysis of retinal sections. VEGF was consistently detected in retinal neurons (closed arrowheads in D–G), although its expression decreased at P28 (open arrowheads in H). Abundant VEGF proteins were detected in the outer segments of P28 eyes (arrows in H). VEGFR2 expression in the embryonic day 17.5 (E17.5) retina is much weaker than that in the postnatal retinas (open arrowheads in M). (Q and R) Whole-mount retinas. (S) Quantitative PCR analysis of peripheral retinas at P2 (n = 4). Bars: (I–L) 500 µm; (D–H and M–R) 50 µm. *, $P < 0.05$; two-tailed Student's t tests. Representative confocal images from three independent experiments (three mice per group) are shown. Data are represented as mean ± SD.

Planck Institute for Biophysical Chemistry, Göttingen, Germany; Marquardt et al., 2001) were mated with *Vegfa-flox* mice (Genentech; Gerber et al., 1999) and/or *Vegfr2-flox* mice (Okabe et al., 2014) to obtain neuron-specific *Vegfa* and/or *Vegfr2* knockout mice. *Vegfr2*$^{\Delta s/\Delta s}$, *Cdh5-BAC-Cre*^{ERT2} (Okabe et al., 2014), *Vegfr1-BAC-DsRed*, *Vegfr2-BAC-EGFP* (Ishitobi et al., 2010), *Vegfr2-DMME-EGFP*, and *Vegfr2*$^{\Delta DMME/\Delta DMME}$ mice were previously described (Ishitobi et al., 2011). 40 µg 4-hydroxytamoxifen was subcutaneously injected at the indicated time. Littermates were used as controls. All aforementioned mice were maintained on a C57BL/6J background.

Preparation of retinal sections. Enucleated eyes were fixed for 10 min in 4% paraformaldehyde in PBS, and then hemispheres were cut. After overnight postfixation, samples were snap frozen in optimal cutting temperature compound (Sakura). All specimens were sectioned 10–60 µm thick at the plane of the optic disk.

Preparation of whole-mount hyaloid vessels and retinas. Enucleated eyes were fixed for 20 min in 4% paraformaldehyde in PBS and then dissected. A small hole was made in the cornea using a 27-gauge needle, and a circular incision was made using fine scissors. After removal of the lenses through

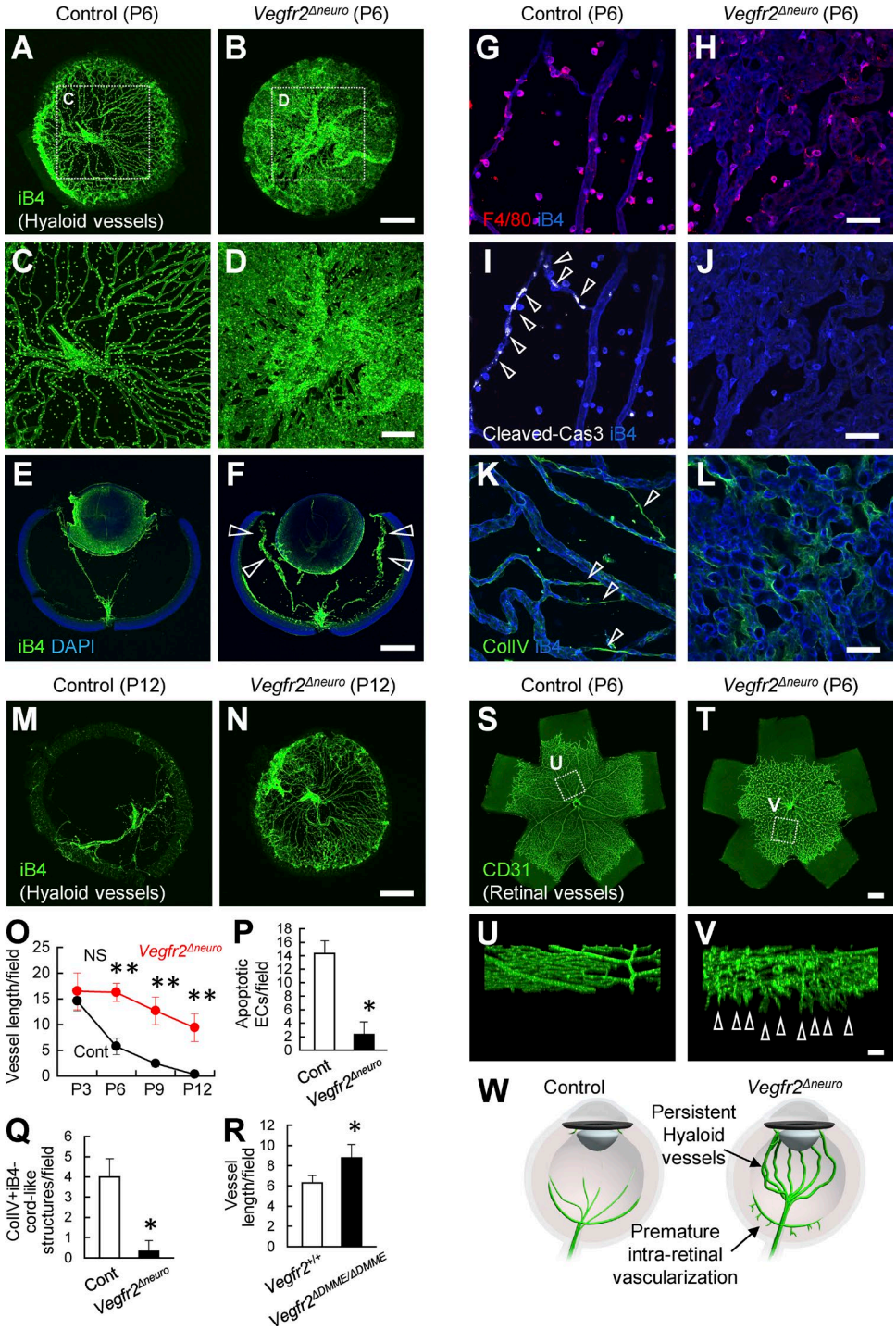

Figure 4. **Lack of neuronal VEGFR2 leads to persistent hyaloid vessels.** (A–R) Whole-mount or section staining of hyaloid vessels at P6 or P12 and quantification ($n = 4$). The amount of hyaloid vessels is increased in *Vegfr2*$^{\Delta neuro}$ mice (arrowheads in F). The abundant endothelial apoptosis (arrowheads in I) and vessel regression (arrowheads in K) detected in control mice are greatly reduced in *Vegfr2*$^{\Delta neuro}$ mice. (S–V) Whole-mount staining of the retinal vasculature. Premature intraretinal vascularization (arrowheads in V) are seen in *Vegfr2*$^{\Delta neuro}$ mice. (W) Schematic diagram depicting vascular abnormalities in *Vegfr2*$^{\Delta neuro}$ mice. Bars: (A, B, E, F, M, N, S, and T) 500 µm; (C, D, U, and V) 200 µm; (G–L) 50 µm. *, $P < 0.05$; **, $P < 0.01$; two-tailed Student's *t* tests. Representative confocal images from four independent experiments (four mice per group) are shown. Data are represented as mean ± SD. ECs, endothelial cells; CollV, collagen type four; Cont, control.

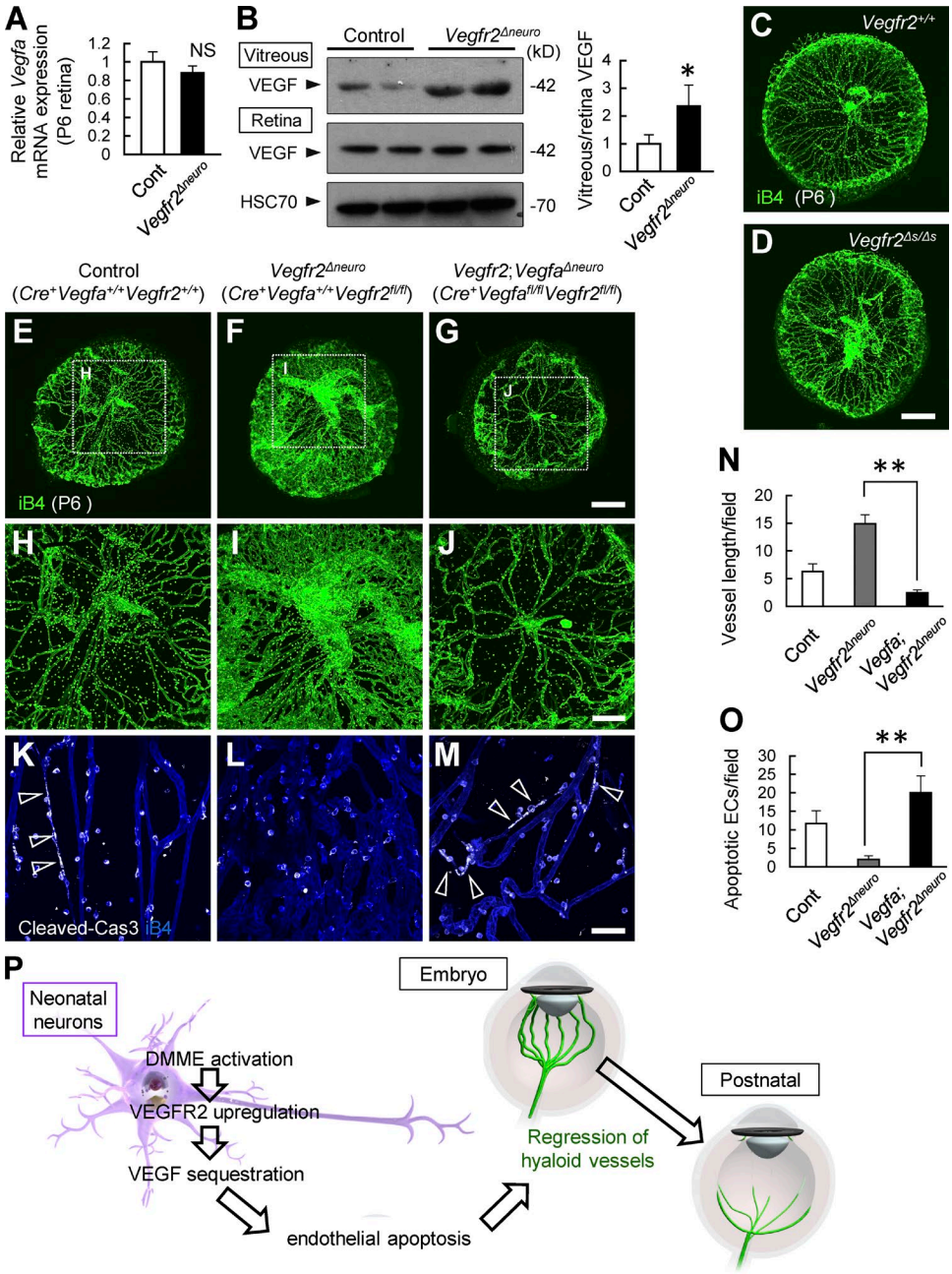

Figure 5. **Deletion of VEGF normalizes persistent hyaloid vessels in neuronal VEGFR2 knockout mice.** (A) Quantitative PCR analysis for retinal tissues at P6 ($n = 4$). (B) Representative immunoblots and quantification in three independent experiments. (C–O) Whole-mount staining of hyaloid vessels at P6 and quantification ($n = 4$). Spontaneous endothelial apoptosis detected in control mice (arrowheads in K) is greatly reduced in *Vegfr2*$^{\Delta neuro}$ mice and is recovered in *Vegfr2*;*Vegfa*$^{\Delta neuro}$ mice (arrowheads in M). (P) Schematic diagram depicting the transition of ocular circulatory systems. Bars: (C–G) 500 µm; (H–J) 200 µm; (K–M) 50 µm. *, $P < 0.05$; **, $P < 0.01$; two-tailed Student's *t* tests. Representative confocal images from four independent experiments (four mice per group) are shown. Data are represented as mean ± SD. Cont, control; ECs, endothelial cells.

the pupils, hyaloid vessels were isolated en bloc with the iris, which acted as a frame. After that, retinal cups were dissected as described previously (Kubota et al., 2009). The whole-mount tissues were postfixed for 30 min and then stained as described in the following section.

Whole-mount immunostaining. Immunohistochemistry of whole-mount samples or tissue sections was performed as previously described (Kubota et al., 2009). The primary monoclonal antibodies used were hamster anti-CD31 (MAB1398Z; EMD Millipore), PDGFRα (14-1401; eBiosci-

ence), vascular endothelial cadherin (550548; BD), and F4/80 (MCA497R; Serotec). The primary polyclonal antibodies used were Alexa Fluor 488–conjugated anti-GFP (A21311; Molecular Probes), collagen IV (LSL-LB-1407; Cosmo Bio), anti-VEGF (sc-152; Santa Cruz Biotechnology, Inc.), and cleaved caspase-3 (9664; Cell Signaling Technology). The secondary antibodies used were Alexa Fluor 488 fluorescence–conjugated IgGs (Molecular Probes) or Cy3/Cy5 DyLight 549/DyLight 649–conjugated IgGs (Jackson ImmunoResearch Laboratories, Inc.). For nuclear staining, specimens were treated with DAPI (Molecular Probes). In some experiments, blood vessels and monocyte lineage cells were simultaneously visualized using biotinylated isolectin B4 (B-1205; Vector Laboratories) followed by fluorescent streptavidin conjugates (Molecular Probes).

Confocal microscopy. Fluorescent images were obtained using a confocal laser-scanning microscope (FV1000; Olympus). Quantification of cells or substances of interest was conducted on a 500 × 500–µm field for vessel length or a 300 × 300–µm field for the number of macrophages, apoptotic cells, and collagen $IV^{+}iB4^{-}$ cord-like structures per sample in scanned images. Multiple slices horizontally imaged from the same field of view at 0.5-µm intervals were integrated to construct three-dimensional images using an FV10-ASW Viewer (Olympus).

Intraocular injections. Injections into the vitreous body were performed using 33-gauge needles, as described previously (Okabe et al., 2014). 0.5 µl sterile PBS with or without 0.1 mg/ml Flt1-Fc chimera proteins (R&D Systems) was injected at P4.

Western blotting. Western blot analysis was performed as described previously (Okabe et al., 2014). The primary antibodies used were anti-VEGF (sc-152; Santa Cruz Biotechnology, Inc.) and HSC 70 (sc-7298; Santa Cruz Biotechnology, Inc.). The fluids of the vitreous cavity were harvested by rinsing posterior segments of eyeballs with PBS and then thoroughly removing the few cellular components via centrifugation.

Quantitative RT-PCR analysis. Total RNA was prepared from retinal tissues, and reverse transcription was performed using Superscript II (Invitrogen). Quantitative PCR assays were conducted with a real-time PCR system (ABI 7500 Fast) using PCR master mix (TaqMan Fast Universal; Applied Biosystems) and a TaqMan gene expression assay mix of *vegfa* (Mm00437304_ml) and *vegfr2* (Mm00440099_ml). A mouse *β-actin* (Mm00607939_s1) assay mix served as an endogenous control. Data were analyzed using SDS software (1.3.1.; 7500 Fast System). Each experiment was performed with four replicates from each sample, and the results were averaged.

Statistics. Results are expressed as the mean ± SD. The comparisons between the means of the two groups were evaluated using a two-tailed Student's *t* test. P-values <0.05 were considered statistically significant.

ACKNOWLEDGMENTS

We thank Naoko Numata for her technical support.

This work was supported by grants-in-aid for Scientific Research on Innovative Areas from the Ministry of Education, Culture, Sports, Science, and Technology of Japan (22122002) and by a research grant from the Senri Life Science Foundation, the Uehara Memorial Foundation, The Tokyo Biochemical Research Foundation, Kowa Life Science Foundation, Ichiro Kanehara Foundation for the Promotion of Medical Sciences and Medical Care, The Yasuda Medical Foundation, Saigh Foundation, Sumitomo Foundation, Suzuken Memorial Foundation, Toray Science Foundation, and Nakatomi Foundation.

The authors declare no competing financial interests.

Submitted: 17 December 2015
Accepted: 6 May 2016

REFERENCES

Albuquerque, R.J., T. Hayashi, W.G. Cho, M.E. Kleinman, S. Dridi, A. Takeda, J.Z. Baffi, K. Yamada, H. Kaneko, M.G. Green, et al. 2009. Alternatively spliced vascular endothelial growth factor receptor-2 is an essential endogenous inhibitor of lymphatic vessel growth. *Nat. Med.* 15:1023–1030. http://dx.doi.org/10.1038/nm.2018

Ambati, B.K., M. Nozaki, N. Singh, A. Takeda, P.D. Jani, T. Suthar, R.J. Albuquerque, E. Richter, E. Sakurai, M.T. Newcomb, et al. 2006. Corneal avascularity is due to soluble VEGF receptor-1. *Nature.* 443:993–997. http://dx.doi.org/10.1038/nature05249

Gerber, H.P., K.J. Hillan, A.M. Ryan, J. Kowalski, G.A. Keller, L. Rangell, B.D. Wright, F. Radtke, M. Aguet, and N. Ferrara. 1999. VEGF is required for growth and survival in neonatal mice. *Development.* 126:1149–1159.

Ishitobi, H., K. Matsumoto, T. Azami, F. Itoh, S. Itoh, S. Takahashi, and M. Ema. 2010. Flk1-GFP BAC Tg mice: an animal model for the study of blood vessel development. *Exp. Anim.* 59:615–622. http://dx.doi.org/10.1538/expanim.59.615

Ishitobi, H., A. Wakamatsu, F. Liu, T. Azami, M. Hamada, K. Matsumoto, H. Kataoka, M. Kobayashi, K. Choi, S. Nishikawa, et al. 2011. Molecular basis for Flk1 expression in hemato-cardiovascular progenitors in the mouse. *Development.* 138:5357–5368. http://dx.doi.org/10.1242/dev.065565

Kubota, Y., K. Takubo, T. Shimizu, H. Ohno, K. Kishi, M. Shibuya, H. Saya, and T. Suda. 2009. M-CSF inhibition selectively targets pathological angiogenesis and lymphangiogenesis. *J. Exp. Med.* 206:1089–1102. http://dx.doi.org/10.1084/jem.20081605

Kurihara, T., Y. Kubota, Y. Ozawa, K. Takubo, K. Noda, M.C. Simon, R.S. Johnson, M. Suematsu, K. Tsubota, S. Ishida, et al. 2010. von Hippel-Lindau protein regulates transition from the fetal to the adult circulatory system in retina. *Development.* 137:1563–1571. http://dx.doi.org/10.1242/dev.049015

Lang, R.A., and J.M. Bishop. 1993. Macrophages are required for cell death and tissue remodeling in the developing mouse eye. *Cell.* 74:453–462. http://dx.doi.org/10.1016/0092-8674(93)80047-I

Lobov, I.B., S. Rao, T.J. Carroll, J.E. Vallance, M. Ito, J.K. Ondr, S. Kurup, D.A. Glass, M.S. Patel, W. Shu, et al. 2005. WNT7b mediates macrophage-induced programmed cell death in patterning of the vasculature. *Nature.* 437:417–421. http://dx.doi.org/10.1038/nature03928

Marquardt, T., R. Ashery-Padan, N. Andrejewski, R. Scardigli, F. Guillemot, and P. Gruss. 2001. Pax6 is required for the multipotent state of retinal progenitor cells. *Cell.* 105:43–55. http://dx.doi.org/10.1016/S0092-8674(01)00295-1

Muranishi, Y., K. Terada, T. Inoue, K. Katoh, T. Tsujii, R. Sanuki, D. Kurokawa, S. Aizawa, Y. Tamaki, and T. Furukawa. 2011. An essential role for RAX

homeoprotein and NOTCH-HES signaling in Otx2 expression in embryonic retinal photoreceptor cell fate determination. *J. Neurosci.* 31:16792–16807. http://dx.doi.org/10.1523/JNEUROSCI.3109-11.2011

Okabe, K., S. Kobayashi, T. Yamada, T. Kurihara, I. Tai-Nagara, T. Miyamoto, Y.S. Mukouyama, T.N. Sato, T. Suda, M. Ema, and Y. Kubota. 2014. Neurons limit angiogenesis by titrating VEGF in retina. *Cell.* 159:584–596. http://dx.doi.org/10.1016/j.cell.2014.09.025

Potente, M., H. Gerhardt, and P. Carmeliet. 2011. Basic and therapeutic aspects of angiogenesis. *Cell.* 146:873–887. http://dx.doi.org/10.1016/j.cell.2011.08.039

Rao, S., C. Chun, J. Fan, J.M. Kofron, M.B. Yang, R.S. Hegde, N. Ferrara, D.R. Copenhagen, and R.A. Lang. 2013. A direct and melanopsin-dependent fetal light response regulates mouse eye development. *Nature.* 494:243–246. http://dx.doi.org/10.1038/nature11823

Rattner, A., Y. Wang, Y. Zhou, J. Williams, and J. Nathans. 2014. The role of the hypoxia response in shaping retinal vascular development in the absence of Norrin/Frizzled4 signaling. *Invest. Ophthalmol. Vis. Sci.* 55:8614–8625. http://dx.doi.org/10.1167/iovs.14-15693

Saint-Geniez, M., A.E. Maldonado, and P.A. D'Amore. 2006. VEGF expression and receptor activation in the choroid during development and in the adult. *Invest. Ophthalmol. Vis. Sci.* 47:3135–3142. http://dx.doi.org/10.1167/iovs.05-1229

Sapieha, P., M. Sirinyan, D. Hamel, K. Zaniolo, J.S. Joyal, J.H. Cho, J.C. Honoré, E. Kermorvant-Duchemin, D.R. Varma, S. Tremblay, et al. 2008. The succinate receptor GPR91 in neurons has a major role in retinal angiogenesis. *Nat. Med.* 14:1067–1076. http://dx.doi.org/10.1038/nm.1873

Silbert, M., and A.S. Gurwood. 2000. Persistent hyperplastic primary vitreous. *Clin. Eye Vis. Care.* 12:131–137. http://dx.doi.org/10.1016/S0953-4431(00)00054-0

Usui, Y., P.D. Westenskow, T. Kurihara, E. Aguilar, S. Sakimoto, L.P. Paris, C. Wittgrove, D. Feitelberg, M.S. Friedlander, S.K. Moreno, et al. 2015. Neurovascular crosstalk between interneurons and capillaries is required for vision. *J. Clin. Invest.* 125:2335–2346. http://dx.doi.org/10.1172/JCI80297

Wang, Y., A. Rattner, Y. Zhou, J. Williams, P.M. Smallwood, and J. Nathans. 2012. Norrin/Frizzled4 signaling in retinal vascular development and blood brain barrier plasticity. *Cell.* 151:1332–1344. http://dx.doi.org/10.1016/j.cell.2012.10.042

Xu, Q., Y. Wang, A. Dabdoub, P.M. Smallwood, J. Williams, C. Woods, M.W. Kelley, L. Jiang, W. Tasman, K. Zhang, and J. Nathans. 2004. Vascular development in the retina and inner ear: control by Norrin and Frizzled-4, a high-affinity ligand-receptor pair. *Cell.* 116:883–895. http://dx.doi.org/10.1016/S0092-8674(04)00216-8

Ye, X., Y. Wang, and J. Nathans. 2010. The Norrin/Frizzled4 signaling pathway in retinal vascular development and disease. *Trends Mol. Med.* 16:417–425. http://dx.doi.org/10.1016/j.molmed.2010.07.003